On the Photo- and Cathodoluminescence of LaB₃O₆:Gd,Bi, Y₃Al₅O₁₂:Pr, Y₃Al₅O₁₂:Gd, Lu₃Al₅O₁₂:Pr, and Lu₃Al₅O₁₂:Gd

Michael Laube, [1,z] **Daniel den Engelsen,** [2] **Thomas Jansen,** [1] **George Fern,** [2] **Paul Harris,** [2] **Terry Ireland,** [2] **Jack Silver,** [2] **and Thomas Jüstel** [1]

¹*Research Group Tailored Optical Materials, Department of Chemical Engineering, University of Applied Sciences Münster, D-48565 Steinfurt, Germany*
²*Centre for Phosphor and Display Materials, Wolfson Centre for Materials Processing, Brunel University London, Uxbridge, Middlesex UB8 3PH, United Kingdom*

Y₃Al₅O₁₂ (YAG) and Lu₃Al₅O₁₂ (LuAG) doped with rare earth elements are widely used as scintillators, solid state lasers, and phosphors in white light emitting diodes (LEDs). Additionally, (Gd,La)B₃O₆:Bi has found application as a UV-B emitting phosphor in fluorescent lamps a long time ago. This paper reports both the photoluminescence (PL) and cathodoluminescence (CL) of Pr^{3+} or Gd^{3+} substituted YAG and LuAG in comparison to the widely applied UV-B phosphor (Gd,La)B₃O₆:Bi under vacuum ultra violet (VUV) and cathode ray excitation, respectively. The powder diffraction pattern, emission, excitation, and reflection spectra and a comparison of the luminescence efficiency are shown and discussed. It turned out that all investigated phosphors show efficient luminescence in the UV-B spectral range. Moreover, it is found that LuAG:Gd has the highest efficiency upon VUV and upon CL excitation too.

Since the early 20ᵗʰ century, there has been much progress in developing phosphors for a wide variety of applications including lighting, displays, marking, coding and medical applications. Amongst the latter phosphors, ultraviolet (UV) emitting phosphors are in high demand for fluorescent lamps that are used in the medical treatment of psoriasis or vitiligo, parapsoriasis, atopic dermatitis, mycosis and fungoides. They also find use in everyday life (for tanning), in chemistry (for photochemistry) and in the UV curing of polymers. Although UV-A (315 nm < λ < 400 nm) light emitting diodes (UVLEDs) have already made great progress in terms of efficiency and lifetimes,[1] UV-B (280 nm < λ < 315 nm) and UV-C (λ < 280 nm) emitting LEDs are not commercially available; this is due to their limited lifetime (lower than a few thousand hours and their relatively low efficiency).[2,3] Consequently, mercury vapor discharge lamps are still in use for such applications. However, these lamps have some shortcomings; including long ignition times due to the delayed evaporation of the mercury, fast aging of the lamps (which results in poor lifetimes), typically less than 10,000 h and restrictions in the lamp geometry.

Therefore, alternative lamp designs, e.g. based on excimer discharges or cathode luminescence are still being actively pursued. For these excitation mechanisms efficient UV phosphors are required.

VUV radiation or electrons can be used to excite a luminescent material. In most cases the host material is substituted with an activator ion. In the past Tl^+, Pb^{2+}, or Bi^{3+} were often used for UV emitting phosphors like NH₄Cl:Tl⁺,[4] BaSi₂O₅:Pb²⁺[5] and YPO₄:Bi³⁺.[6,7] Currently one uses more often non-hazardous rare earth elements such as cerium in LaPO₄:Ce³⁺[8], praseodymium in Y₃Al₅O₁₂:Pr³⁺,[9] gadolinium in (Gd,La)B₃O₆:Bi³⁺[10,11] as activator ions for UV emitting phosphors. Another possible field of application is in scintillator materials. Here the fast (allowed) transition of Ce^{3+} or Pr^{3+} is used to convert high energy photons into the UV or visible (VIS) range of the electromagnetic spectrum.[12,14,15] Interestingly, activators are not always needed since some materials show intrinsic UV emission, (which is generated by the host itself). The reason can be related to exciton emission or defects in the crystal structure (antisite defects) as reported for LuAG and YAG.[13,16,17] They are often applied as single crystalline films,[18] which proves that these garnets are very resistant to high excitation energies. This is especially useful because VUV radiation as well as electrons transfer much energy to the host material. (Gd,La)B₃O₆:Bi is also a well-established UV phosphor, which can be excited with the 254 nm radiation emitted by Hg*.[10,11] The emission line of (Gd,La)B₃O₆:Bi³⁺ peaks at 312 nm which makes it a suitable phosphor for tanning lamps (Philips PL-S 9W/835/2P/ALTO). Although there are many publications concerning UV emitting phosphors, to the best of our knowledge, little to no comparative studies exist for cathode ray and deuterium lamp (λ_{ex} = 160 nm) excited phosphors. This is especially interesting since the luminescent properties often depend on the source of excitation. To this end we have investigated the UV emission of efficient UV-B emitting phosphors excited by VUV radiation and cathode rays (electrons) and found some interesting differences in their emission behavior and intensity which we report herein.

Experimental

***Materials and synthesis.*—**Powder samples of Y₃Al₅O₁₂:Gd³⁺ (1%) (YAG:Gd), Y₃Al₅O₁₂:Pr³⁺(1%) (YAG:Pr), Lu₃Al₅O₁₂:Gd³⁺ (5%) (LuAG:Gd) and Lu₃Al₅O₁₂:Pr³⁺(1%) (LuAG:Pr) were all prepared in a similar way. Stoichiometric amounts of the powdered reactants were carefully weighed with an analytical balance. In a first step, the metal nitrates Al(NO₃)₃·9H₂O (Alfa Aesar, 98–102%) and Pr(NO₃)₃·6H₂O (Alfa Aesar, 99.99%) were dissolved in deionized water. The metal oxides Y₂O₃ (Treibacher, 99.99%), Lu₂O₃ (Treibacher, 99.9%) and Gd₂O₃ (Treibacher, 99.99%) were separately dissolved in concentrated boiling HNO₃ (VWR, AnalaR NORMAPUR, 65%). The metal oxide solution was added to the solution of the dissolved metal nitrates. Afterwards, the fuel tris(hydroxymethyl)aminomethane (VWR, 100,00%) (Tris) was added in a molar ratio of 2:1 in proportion to the metal ions. After concentrating the mixtures by slow evaporation at 80°C, the sols turned into transparent, highly viscous gels. Next, the translucent gel was heated at 300°C until the self-propagating, exothermic combustion process started. This resulted in a black foam, which was dried in an oven at 150°C for 12 h. The black foam was ground in an agate mortar. To get rid of the organic residue, the powder was heated at 900°C for 6 h in air. The received white powders were again ground in an agate mortar and heated at 1600°C for 8 h.

LaB₃O₆:Gd³⁺(10%),Bi³⁺(2%), was prepared by a conventional high temperature solid state method. The powdered reactants H₃BO₃ (Merck, 99.5 – 100.5%), Gd₂O₃ (Treibacher, 99.99%), La₂O₃ (Treibacher, 99.995%), and Bi(NO₃)₃·5H₂O (98%) were weighed with an analytical balance and put into an agate mortar. After adding a few millilitres of acetone, the powders were mixed thoroughly. The dried mixture was transferred to a corundum crucible and heated at 900°C for 4 h. The white powder was ground and fired again in the same

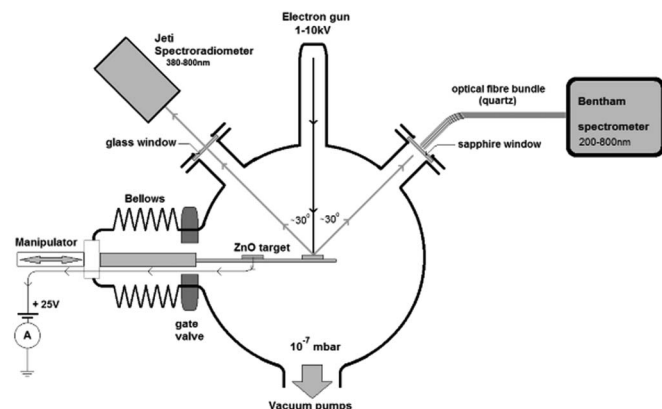ᶻE-mail: michael.laube@fh-muenster.de

Figure 1. Schematic view of the vacuum system and spectrometer arrangement.

corundum crucible at 1000°C for 8 h. Crystallinity and phase purity of all products were checked by X-ray powder diffraction (XRPD).

Cathodoluminescence measurements.—Figure 1 displays the vacuum system and arrangement of the spectrometers for the cathodoluminescence (CL) measurements. The residual pressure in the vacuum system during the CL measurements was between 1×10^{-7} mbar and 1×10^{-6} mbar. A Staib ES 1059 electron gun, which could be operated between 500 V and 10 kV, was used to generate the electron (e) beam. We used a defocussed static E-beam at 8 kV for this work and the average current density in electron spot was 3.75 µA/cm² for the UV phosphors and the calibration phosphor ZnO:Zn. The CL spectra were recorded with a Bentham M300 monochromator between 210 and 800 nm using two gratings: for the low wavelengths between 210 and 600 nm we used a grating with 2400 grooves/mm (blazed at 250 nm) and for the wavelengths > 600 nm we used a grating with 1200 grooves/mm (blazed at 500 nm). The resolution of the monochromator was about 0.5 nm, while the absolute accuracy of the wavelength scale was about ±1 nm. The recording of CL spectra is a standard measuring technique since electron guns became commercially available in the last century. However, the determination of the energy efficiency and luminous efficacy of CL is not straight forward because of the charging of the phosphors and emission of secondary electrons. In order to cope with these problems, we have developed a new technique, which we coined "the comparison method".[19,20] In the comparison method we apply a non-charging phosphor (ZnO:Zn) to calibrate the radiance measurements of the Bentham spectrometer in arbitrary units to W/(sr m²)-units and to adjust the effective current density on the charging phosphors. The details of this method have been described in Refs. 21,19. We have applied this method for the determination of the energy efficiency of the CL of the phosphors mentioned in the experimental section.

The window between the quartz fiber bundle (connected to the Bentham spectrometer) and the vacuum was sapphire. The other window of glass was used to monitor the radiance of ZnO:Zn in the visible part of the spectrum. The spectral radiance of this material was measured in W/(sr m² nm) with a Jeti Radiometer (Spectrobos 1200) between 380 and 780 nm.

The phosphor powders were applied to an Al-strip as described previously[22] and could be manoeuvred into the E-beam by horizontal translation and adjusting the azimuth. The secondary emitted electrons were captured on the conducting ZnO target by biasing it at 25 V. The ZnO phosphor layer was electrically insulated from the grounded Al-strip containing the non-conducting UV-phosphors.

X-ray powder diffraction.—Phase formation, purity and crystallinity were determined using a Rigaku MiniFlex II diffractometer. The diffractometer was operated in Bragg-Brentano ($\Theta/2\Theta$) geometry with Cu-K$_\alpha$ radiation (0.154 nm) as X-ray source. Typically, the

powder diffraction patterns were measured from 10 to 80°. The step width was set to 0.02°.

Diffuse reflection spectra.—Diffuse reflection spectra were recorded on a FS 920 (Edinburgh Instruments) spectrometer, which used a Xe arc lamp (450 W) for excitation. The sample was placed in an integration sphere coated with optical PTFE (Spectralon). A −20°C cooled single photon multiplier (Hamamatsu R928) was used as a detector. For calibration the measured reflection spectra were divided by the reflection spectrum of BaSO₄ (Sigma Aldrich, 99.998%).

Photoluminescence spectroscopy.—For the UV emission measurements, a FS 920 VUV spectrometer form Edinburgh Instruments was used. The excitation arm consisted of an evacuated (p ≈ 3.4 × 10^{-6} mbar) VUV monochromator (VM-504) from Acton Research. For VUV excitation a 30 W deuterium discharge lamp ($\lambda_{ex} = 160$ nm) from Hamamatsu (DS-775) was applied. For emission measurements a grating with 1200 grooves per mm (g/mm) was used, whereas for the excitation measurements a grating with 2400 g/mm was used. The dwell time was typically set to 0.5 s. The slits were set to 0.25 nm for emission measurement and 1.0 nm for the excitation measurement. The sample chamber was constantly flooded with nitrogen to avoid absorption of VUV radiation by water, oxygen and carbon dioxide.

Different optical filters were used to absorb the second order emission of the excitation beam for emission measurements > 400 nm. Therefore, the measurement was split into three parts. The first part was measured from 200 to 400 nm without a filter. For the second part (350–600 nm) a 350 nm long pass filter was used while for the third part (550 – 800 nm) a 550 nm long pass filter was used. The detection arm consisted of a collection lens, a Czerny-Tuner Optics TMS300 monochromator with an 1800 g/mm grating and a photomultiplier tube from Hamamatsu (PMT R928). For emission detection, single photon counting mode was used. During the measurement, the detector was constantly kept at −20°C by Peltier cooling. The slit of the emission arm was set to 1.0 nm for emission and excitation measurements.

Results and Discussion

Phase identification.—In Figure 2 the XRPD patterns of all samples are shown. YAG and LuAG are well known oxides, which belong to the garnet family. The general structure class of garnets is described as $^{[8]}X_3^{[6]}Y_2^{[4]}ZO_4]_3$. Here the Lu³⁺ or Y³⁺ cations occupy X-places, which are dodecahedrally coordinated by oxygen atoms (CN = 8), forming a polyhedron with point symmetry D_2. All garnets possess the same space group viz. **Ia3̄d**. The Al³⁺ cations are located on the Y-sites and Z-sites, which are octahedrally (C_{3i} point symmetry) and tetrahedrally coordinated by oxygen ions.[23] Y³⁺/Lu³⁺ was partially substituted by Gd³⁺ and Pr³⁺ because of their matching ionic radii and charges. For an eight coordinate site the radii are 1.117 Å for Lu³⁺, 1.159 Å for Y³⁺, 1.193 Å for Gd³⁺ and 1.266 Å for Pr³⁺.[24] While the structure shows many similarities, the densities of the materials differ: LuAG has the higher density of 6.69 g/cm³ and YAG only has a density of 4.56 g/cm³.

(Gd,La)B₃O₆:Bi³⁺ is a borate; it crystallizes in the monoclinic crystal system and has the space group $C12/c1$. Here the La³⁺ is surrounded by 9 oxygen atoms (CN = 9). The La³⁺ was partially substituted by Gd³⁺ because of the matching ionic radii in 9 fold coordination. These are 1.247 Å for Gd³⁺, 1.356 Å for La³⁺.[24] Compared to YAG and LuAG its density (4,22 g/cm³) is lower.[25]

CL measurements.—Figure 3a presents the CL spectrum of (Gd,La)B₃O₆:Bi³⁺ between 210 and 600 nm; outside this range we did not detect CL.

The inset of Figure 3b shows the CL spectrum of YAG:Pr at 8 kV between 210 and 800 nm recorded with the 2400 g/mm grating; the enlarged part of the spectrum is the region between 290 and 450 nm. The CL-spectrum of YAG:Pr measured by Gorbenko et al. at 9 keV[26] deviates from the spectrum shown in Figure 3b in our case the spectral radiance of the peaks at 487 nm is much larger than the
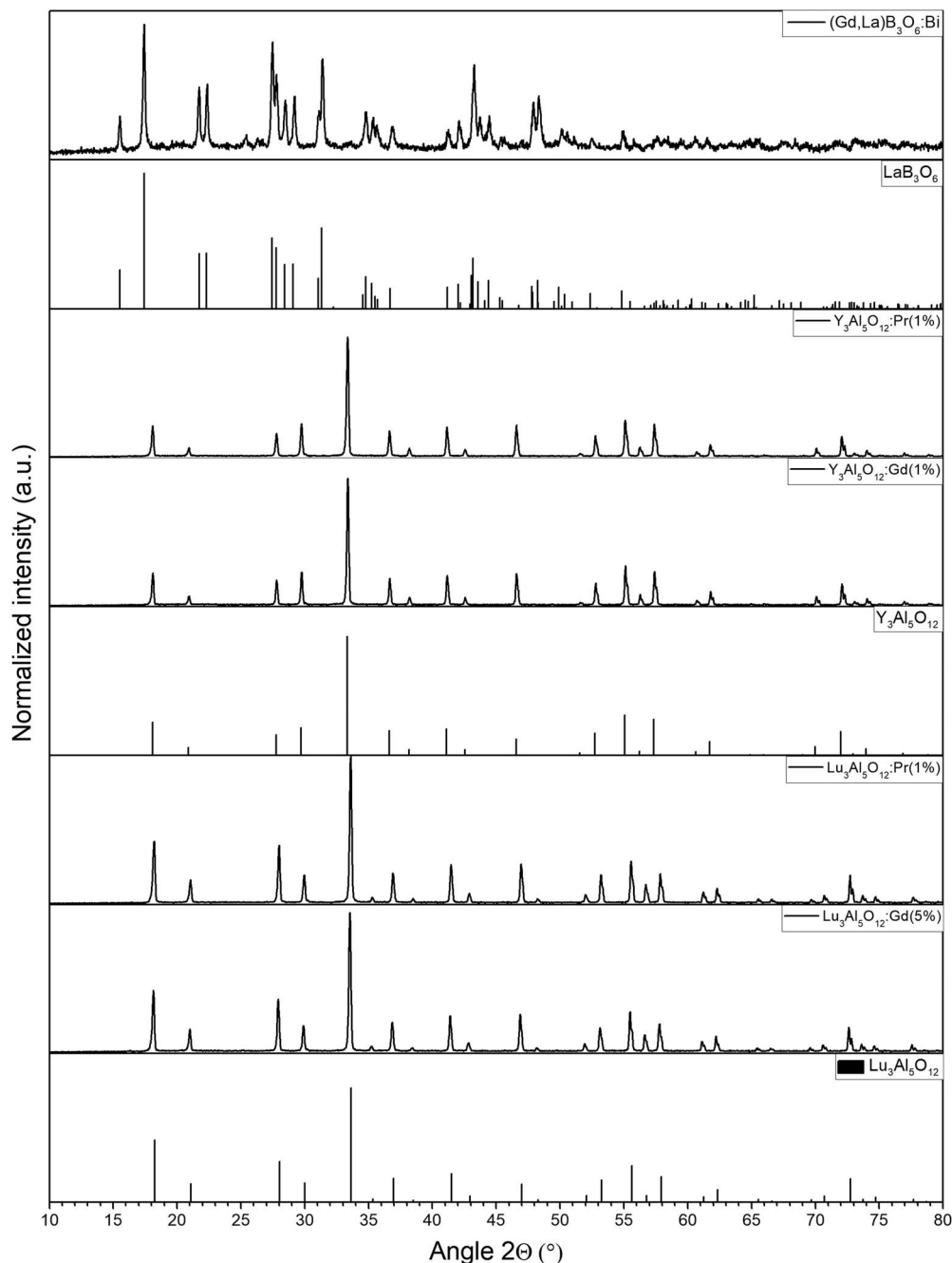
Figure 2. X-ray diffraction pattern of the powdered samples and the reference patterns of LaB_3O_6, $Y_3Al_5O_{12}$ and $Lu_3Al_5O_{12}$.[39,44,45]

radiance measured by them: in other words, we find a much lower radiance in the UV than in the visible region. It should be mentioned that Gorbenko et al.[26] studied single crystalline thin films, which are likely to have different concentrations of defects compared to powders.

Figure 3c is the CL spectrum of YAG:Gd, recorded at 8 kV between 220 and 600 nm. The CL spectrum of YAG:Gd measured by Deng et al.[27] at 5 keV and room temperature also shows the strong emission line at 312 nm. However, their spectrum does not show the broad emission band which can be seen in Figure 3c. The YAG:Gd of Deng et al. was a thin film prepared by reactive sputtering and annealing at 1000°C. We assume that the concentration of defects in their material was also different to those in our material: this could explain the absence of the broad emission peak in their case. This will be discussed in detail hereafter.

Figure 3d shows the CL spectrum of LuAG:Pr at 8 kV between 210 and 800 nm recorded with the 2400 g/mm grating. Gorbenko et al.[26] measured also the CL spectrum (at 9 keV) of LuAG:Pr. They found that the ratio of the spectral radiances at 487 and 307 nm is about 0.1, whereas we find a ratio of about 0.25. For this material we find a lower radiance in the UV region than in the visible. In this case we also need to mention the difference between the type of materials: single crystalline films in the case of Gorbenko et al.,[26] whereas we studied powders.

Figure 3e presents the CL spectrum of LuAG:Gd between 210 and 600 nm. It should be mentioned that the cluster of peaks at 313 nm in Figures 3e has not been saturated. This was checked by recording the spectrum at lower current density: this yielded the correct ratio between the spectral radiances and also the same shape of the spectrum.
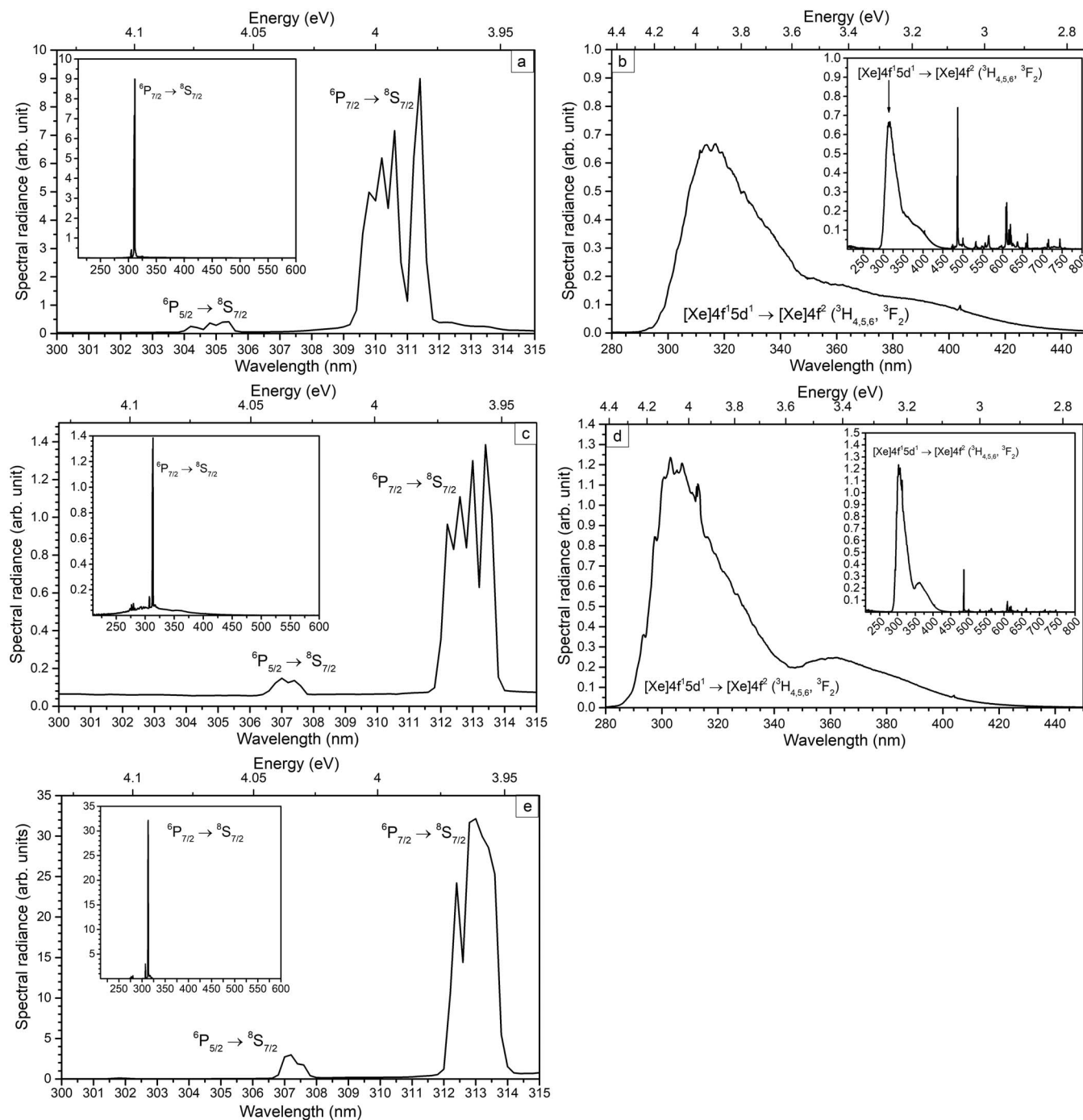
Figure 3. Emission spectrum of $(Gd,La)B_3O_6:Bi^{3+}$ (a), YAG:Pr (b), YAG:Gd (c), LuAG:Pr (d) and LuAG:Gd (e) in the UV-B area, recorded at 8 kV. The inset displays the full-range spectrum of the phosphors measured from 210 to 600 nm $((Gd,La)B_3O_6:Bi^{3+}$, YAG:Gd), 210 to 800 nm (YAG:Pr, LuAG:Pr) and 200 to 600 nm (LuAG:Gd).

From the comparison of Figures 3c and 3e it can be concluded that LuAG:Gd is a much stronger UV emitter than YAG:Gd.

A logarithmic comparison between the spectra of these two phosphors is presented in Figure 4. Apart from the large difference of peak heights at 313 nm, Figures 4 also displays a large difference in background radiation: YAG:Gd shows a broad emission band centred at about 310 nm, whereas this broad emission band is absent in LuAG:Gd. We assume that the broad emission band in YAG:Gd may be assigned to the intrinsic emission of undoped YAG at room temperature.[13,28] Pujāts et al.[28] measured a broad emission band at 310 nm upon excitation of undoped YAG with 8 keV electrons at room temperature, while Babin et al.[13] excited undoped YAG and LuAG with high energy synchrotron radiation and measured a broad emission band at 315 nm at room temperature in YAG and a similar broad emission at 340 nm in LuAG. Intrinsic emission at 310 nm from LuAG:Ce by excitation with an E-beam at room temperature has been reported by Kucera et al.[29] Recently we have studied the intrinsic emission of cubic Y_2O_3 and $Y_2O_3:Eu[21]$ upon excitation with 200 keV electrons. It was found that the intensity of the intrinsic emission in Y_2O_3 is a function of temperature: at room temperature this emission is completely quenched. We also found that doping Y_2O_3 with Eu^{3+} decreases the intrinsic emission strongly.
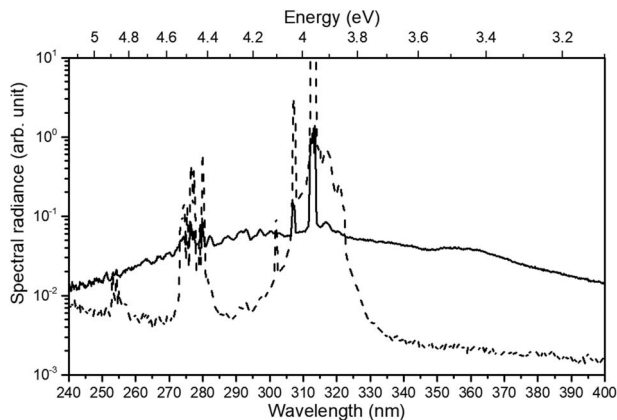
Figure 4. CL spectra of YAG:Gd (solid line) and LuAG:Gd (dashed line) at 8 kV and 3.75 μA/cm^2 represented on a logarithmic scale. The 313 nm peak of LuAG:Gd is more than one order of magnitude larger than the corresponding peak of YAG:Gd.

By comparing Figures 3b and 3d it can be seen that YAG:Pr does not show intrinsic emission in the area from 250 to 400 nm, which leads to the conclusion that in this latter phosphor the transfer of energy from the host lattice to the rare earth ion is easier than in the case of YAG:Gd. The two LuAG-phosphors do not show intrinsic luminescence either, leading to the same conclusion on the energy transfer from host lattice to the rare earth ions.

From the difference in peak heights at 313 nm we expect that the energy efficiency of the UV radiation from LuAG:Gd is more than 10 times larger than that from YAG:Gd. Although one should keep in mind that the doping concentration of Gd^{3+} in LuAG is five times larger than in YAG. This will be considered in the next section, where we shall also discuss the mechanism of the intrinsic emission of YAG and LuAG.

Energy efficiency of the CL.—In this section we shall describe the energy efficiency of the CL of the UV emitting phosphors. The energy efficiency η of the luminescence is the power density of the emitted radiation divided by the power density of the E-beam. Here we shall distinguish between the efficiency of the UV radiation, indicated by η_{UV}, and the efficiency of the visible radiation, indicated by η_{VIS}. The evaluation of η from the spectra by the comparison method has been described before.[7,19,20] As indicated in these publications, we need to assume that the distribution of the CL from the phosphor powders is Lambertian. For the evaluation of η_{UV} we have integrated the spectral radiance SR(λ) between 220 and 400 nm according to

$$R_{UV} = \int_{220}^{400} SR(\lambda)d\lambda \qquad [1]$$

where R_{UV} is the radiance between 220 and 400 nm expressed in W/(sr m^2). For R_{VIS} we used the corresponding equation between 400 and 600 nm. The result is presented in Table I.

As shown in Figures 3b and 3d, the phosphors YAG:Pr and LuAG:Pr also emit beyond 600 nm. This will increase η_{VIS} by 0.2% and 0.1% respectively. As expected from Figures 3c and 3e, η_{UV} of YAG:Gd is smaller by about a factor of 6.5 than η_{UV} of LuAG:Gd. This is a factor of 2 less than what could be expected from the difference in spectral radiance between Figures 3c and 3e. However, the intrinsic emission from YAG:Gd at 310 nm contributes also to η_{UV}, enlarging it by a small amount.

Table I indicates that YAG:Gd is an outlier if the CL efficiency (η_{UV}) is compared to the other YAG and LuAG type phosphors. Its efficiency is only 0.9% while the other phosphors show efficiencies of at least 3.4%. Before turning our attention to the intrinsic emission of YAG and LuAG, the odd behavior of YAG:Gd may also be illustrated

with an empirical formula that describes the CL efficiency as a function of the mean atomic number Z_m of the phosphor.[30] That formula is:

$$\eta_T(\%) = 16.7 Ln Z_m - 25 \qquad [2]$$

It was stressed by Yamamoto that this formula refers to single crystals; for powder layers the efficiencies are much lower.[31]

In Table II we have summarized the CL efficiency for the YAG and LuAG phosphors. The last row of Table II presents the ratio between the efficiencies of the YAG and LuAG phosphors. It can be seen that the phosphors doped with Gd deviate substantially from the behavior predicted by Eq. 2, whereas the efficiencies of the Pr-doped phosphors follow more or less the trend indicated by Eq. 2.

The energy transfer from host lattice to rare earth dopants and the observation of intrinsic emission in YAG:Gd makes the application of the empirical formula (2) precarious.

The study of the intrinsic luminescence from undoped YAG and LuAG remains popular since the development of YAG:Nd scintillators, because of the recent application of co-doped (with Ga or Gd) LuAG and YAG as scintillator materials and the use of YAG:Ce in white LEDs.[30] It was also attributed that the intrinsic emission of YAG and LuAG at 310 nm refers to shallow electrons traps associated with antisite defects, Lu$_{Al}$ or Y$_{Al}$ (a Lu or Y atom at an Al-site), and excitons localized near these defects.[30,32,33] These defects are easily formed in single crystals of Y- and Lu-garnets, as explained by Nikl et al.[30] upon cooling down garnet crystals after preparation at high temperatures. The intensity of the intrinsic emission is assumed to increase upon increasing this defect concentration. Based on this relation, it may be concluded that the concentration of antisite defects in YAG:Pr, LuAG:Pr and LuAG:Gd is low, whereas in YAG:Gd it must be higher. This mechanism is thought to be responsible for the rather inefficient energy transfer from the YAG-lattice to Gd as compared to the corresponding transfer in the other garnets.

Reflection spectra.—The reflection spectra of the samples represent the absorption behavior of the phosphors. While LuAG:Gd, YAG:Gd and (Gd,La)B$_3$O$_6$:Bi^{3+} are white materials with no absorption bands in the visible spectral range, YAG:Pr and LuAG:Pr show absorption bands between 452 and 487 nm as well as between 582 and 611 nm. Due to these absorption bands the materials show a greenish body color. One should also note that (Gd,La)B$_3$O$_6$:Bi^{3+} is not as white as YAG:Gd and LuAG:Gd, which might lead to an increased (re)absorption of the emitted radiation. Furthermore, the reflection

Table I. Energy efficiency of the CL measurements calculated with Equation 1.

	η_{UV}(%)	η_{VIS}(%)	η_T(%)*
(Gd,La)B$_3$O$_6$:Bi^{3+}	1.8	0.1	1.8
YAG:Pr	3.4	0.5	3.9
YAG:Gd	0.9	0.1	1.0
LuAG:Pr	5.5	0.2	5.7
LuAG:Gd	5.8	0.1	5.9
ZnO:Zn		5.4	5.4

*$\eta_T = \eta_{UV} + \eta_{VIS}$.

Table II. Comparison of energy efficiency with values calculated with Eq. 2.

		Theory (Eq. 2)	Experimental (Table I)	
	Z_m	η_T (%)	η_T (%) Gd	η_T (%) Pr
YAG	13.9	18.9	1.0	3.9
LuAG	18.7	23.8	5.9	5.7
Ratio*		0.79	0.17	0.68

*Ratio is the efficiency of the YAG phosphor divided by the efficiency of the LuAG phosphor.

spectrum of $(Gd,La)B_3O_6:Bi^{3+}$ shows a sigmoidal shaped curve. This is partially due to the absorption of Bi^{3+}. Furthermore, the optical bandgap of $(Gd,La)B_3O_6:Bi^{3+}$ was estimated by applying the Tauc function (3):[34,35]

$$[F(R_\infty h\nu)]^n = A(h\nu - E_g) \qquad [3]$$

where $h\nu$ is the photon energy, A is a proportionality constant, E_g is the value of the bandgap, n = 2 for a direct transition or 1/2 for an indirect transition and $F(R_\infty)$ is the Kubelka-Munk function, which is defined as follows (4):[36]

$$F(R_\infty) = \frac{(1-R)^2}{2R} = \frac{K}{S} \qquad [4]$$

where R is the reflection coefficient, K is the absorption coefficient and S is the scattering coefficient. The linear extrapolation $[F(R_\infty h\nu)]^2 = 0$ yields the optical bandgap, which was found to be 4.93 eV (251 nm).

Photoluminescence spectra.—The photoluminescence and reflection spectra of $(Gd,La)B_3O_6:Bi^{3+}$, YAG:Pr^{3+}, YAG:Gd^{3+}, LuAG:Pr^{3+} and LuAG:Gd^{3+} are presented in the Figures 5a, 5b, 5c, 5d and 5e respectively. Due to the different activator ions (Gd^{3+} or Pr^{3+}) the samples show different types of emission when they are excited by VUV radiation of $\lambda_{ex} = 160$ nm or cathode rays with 8 kV. The Gd^{3+} and Bi^{3+} doped materials, YAG:Gd, LuAG:Gd and $(Gd,La)B_3O_6:Bi^{3+}$, show intense line emission peaking at 314 and 312 nm respectively, whilst the Pr^{3+} doped samples, YAG:Pr and LuAG:Pr, show band emission in the UV area as well as line emission in the VIS area. Therefore, the emission of the materials will be discussed in relation to their activators.

Figures 5a, 5c and 5e show the excitation, emission and reflection spectra respectively of the Gd^{3+} doped samples. Although, not all materials show the largest absorption at 160 nm, we used this wavelength for excitation, due to the emission maximum of the D$_2$-lamp. The absorption of the host lattice of the Gd^{3+} doped samples reaches up to 195 nm (6.4 eV). These samples show an excitation band peaking between 270 and 280 nm, which we attribute to the $^8S_{7/2} \rightarrow {}^6I_J$ transition of Gd^{3+}. This is a forbidden transition, which explains why the excitation band is small compared to the excitation of the host, which has its peak around 172 nm (7.2 eV).

The Pr^{3+} doped samples also show host absorption, which reaches up to 200 nm (6.0 eV) and passes over into the first absorption band of Pr^{3+}. The band approaches a maximum at $\sim$ 240 nm (5.2 eV) and is more intense than the excitation intensity of the host lattice. It is assigned to the spin and parity allowed $^3H_4 \rightarrow {}^1S_0$ [Xe]4f^{1}5d^1 transition of Pr^{3+}. In all cases the excitation radiation must be absorbed by the host lattice of the materials, since neither Gd^{3+} nor Pr^{3+} have any known energy levels in the area around 160 nm. In the next step, the energy can be transferred to the ^6P_J energy levels of Gd^{3+} or ^3P_J energy level of Pr^{3+} respectively. One should note that there are other possible trapping and quenching mechanisms in luminescent materials.

The main emission lines of YAG:Gd and LuAG:Gd are peaking between 313 and 315 nm. $(Gd,La)B_3O_6:Bi^{3+}$ also shows this emission line. However, it is shifted to lower wavelength (higher energy and peaks between 310 and 312 nm. We attribute this emission line to the spin- and parity forbidden $^6P_{7/2} \rightarrow {}^8S$ transition of Gd^{3+}. Note that the overview of the VUV excited spectra (Figures 5a, 5c and 5e) was measured with 1 nm steps and emission slit, the spectra in the insets were measured with 0.1 nm steps and emission slit. Thanks to the higher resolution, the splitting of the emission line into four smaller lines becomes visible, which is an effect of the crystal field splitting. One can argue that the f-orbitals of the lanthanide ions normally don't contribute to the binding with the ligands since they are screened by higher energy orbitals like the 5s^2 and 5p^6 orbitals. But since the symmetry is not perfect, f-orbitals always mix with their surrounding orbitals. As a result, the 4f-4f transition becomes allowed.[37,38] This effect is more distinctive in $(Gd,La)B_3O_6:Bi^{3+}$ which shows a crystal field splitting of 287 cm^{-1}, while LuAG:Gd and YAG:Gd only show a difference of 210 cm^{-1} and 220 cm^{-1} respectively.

The different positions of the emission lines of LuAG:Gd or YAG:Gd and $(Gd,La)B_3O_6:Bi^{3+}$ can be explained by considering the different crystal structure and chemical environment of the Gd^{3+} activator ion. In structure of $(Gd,La)B_3O_6:Bi^{3+}$ Gd^{3+} (C12/c1) the Gd^{3+} is on the La^{3+} sites, which are surrounded by 12 oxygen atoms (Z = 12). In LuAG and YAG Gd^{3+} is positioned at the Lu^{3+} and Y^{3+} sites, which are each surrounded by 8 oxygen atoms (Z = 8). Due to the different chemical environment the bond lengths between the Gd^{3+} ion and the O-atom are shorter in LuAG (0.2283-0.2276 nm) than in $(Gd,La)B_3O_6:Bi^{3+}$ (0.2429-0.2846 nm).[39] This results in a higher covalent character of the Gd^{3+} ion in LuAG, which leads to a shift to longer wavelengths (lower energies). The same applies to the second emission band, which can be seen around 305 or 308 nm in $(Gd,La)B_3O_6:Bi^{3+}$ or LuAG:Gd respectively. When looking closer at the spectra, a second smaller emission band between 307 and 309 nm in YAG:Gd and LuAG:Gd and between 304 and 306 nm in $(Gd,La)B_3O_6:Bi^{3+}$ can be seen. We assign this band to the $^6P_{5/2} \rightarrow {}^8S$ transition of Gd^{3+} for the three phosphors. Since we measured the samples at room temperature (RT), thermal population of the $^6P_{5/2}$ level can be excluded. According to Boltzmann statistics more than 860 K would be required to overcome the difference of 600 cm^{-1}. A more likely approach is the incomplete transfer of the electrons from the upper ^6I_J energy levels to the $^6P_{7/2}$ energy level with a subsequent emission from this energy level. Moreover, the difference between the emission lines peaking at 307 and 314 nm ($^6P_{5/2}$ and $^6P_{7/2}$, energy levels) in YAG:Gd or LuAG:Gd and at 304.5 and 312.5 nm in $(Gd,La)B_3O_6:Bi^{3+}$ gives some insight into the spin orbit coupling of the activator ion. Therefore, we calculated the energy difference between the end of the higher energy and beginning of the lower energy emission band. For LuAG:Gd and YAG:Gd this difference is 4.2 nm (0.0541 eV, 435.9 cm^{-1}), while the difference in $(Gd,La)B_3O_6:Bi^{3+}$ is 3.2 nm (0.04193 eV, 338 cm^{-1}). This shows that there is approximately the same energy difference between the $^6P_{5/2}$ and $^6P_{7/2}$ energy levels of Gd^{3+} in the aluminate and borate host material.

The emission spectra of YAG:Pr and LuAG:Pr can be seen in Figures 5b and 5d. The first emission band of YAG:Pr and LuAG:Pr begins in the UV at 290 nm and reaches into the visible part of the electromagnetic spectra to 440 nm. This emission band has been attributed to the [Xe]4f^{1}5d$^1 \rightarrow$ [Xe]4f^2 ($^3H_4$, $^3H_5$) transition of the Pr^{3+} ion.[40,41] Interestingly, this UV emission is more intense in LuAG:Pr than it is in YAG:Pr. In contrast to the Gd^{3+} doped samples, YAG:Pr and LuAG:Pr also show emission lines in the visible area between 480 and 680 nm. These lines are well known and belong to the family of 4f-4f transitions of Pr^{3+}.[40-42]

Although the emission lines appear nearly at the same wavelengths in both samples, the 4f-4f transitions of YAG:Pr are more intense than in the LuAG:Pr sample. However, for both phosphors we assign the emission lines to the $^3P_{1,0} \rightarrow {}^3H_4$, $^3P_{1,0} \rightarrow {}^3H_5$ and $^3P_1 \rightarrow {}^3H_6$ transitions of Pr^{3+}. This assignment also applies to the observed emission lines in the CL spectra, presented in Figures 3b and 3d.

Comparison of the VUV excited photoluminescence properties.—In Figures 6a and 6b the emission spectra of the five phosphors under VUV and CL excitation respectively are compared to each other. The insets show the radiances (integrated intensities) as defined in Eq. 1 in the UV-B range of the electromagnetic spectrum. Figure 6a shows that the Pr doped phosphors show the lowest radiances in this range under VUV excitation (green and black line and bar), although the radiance of LuAG:Pr (black line and bar) almost equals that of YAG:Gd (blue line and bar). $(Gd,La)B_3O_6:Bi^{3+}$ (purple line and bar) is the phosphor with the second largest radiance. The most intense UV-B emitting material is LuAG:Gd (red line and bar).

In Figure 6b the UV-B emission and radiance of the same samples under CL excitation are shown. Although their appearance in the spectra might differ by a few nanometers, the emission lines and bands are nearly the same. The crystal field splitting in LuAG:Gd (red line) is not as distinct under CL excitation than it is under VUV
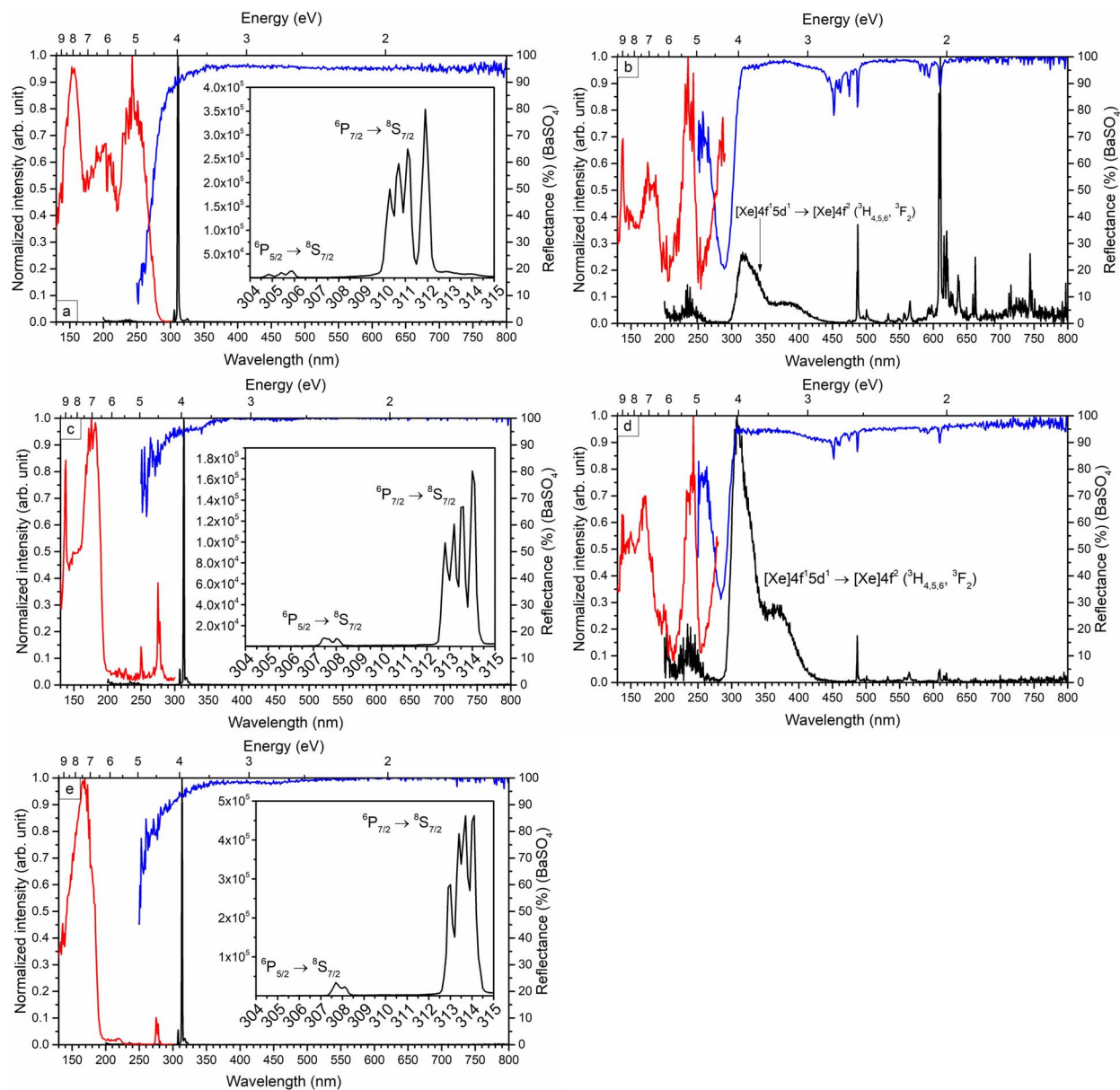
Figure 5. The normalized excitation (red line), emission (black line) and reflection (blue line) spectra of $(Gd,La)B_3O_6:Bi^{3+}$ (a), YAG:Pr (b), YAG:Gd (c), LuAG:Pr (d) and LuAG:Gd (e) are shown respectively. The excitation of the phosphors was measured at 311 nm (a, b), 313.9 nm (c), 309 nm (d) and 313.7 nm (e).

excitation. Note that there is also a difference in the Gd^{3+} doped YAG sample when the sample is excited with electrons: there is a higher background emission between 240 and 400 nm (Figure 4), which we have assigned to the intrinsic emission of undoped YAG, as mentioned above. A possible reason might be an incomplete energy transfer from the host lattice to the activator ion. Interestingly LuAG:Pr, LuAG:Gd and YAG:Pr don't show this behavior under the same excitation conditions. Moreover, the intense luminescence of Gd is not suppressed in YAG:Gd in contrast to the finding of Kucera et al. for Ce^{3+} doped GdGa-LuAG multicomponent garnet films.[29]

In contrast the radiances differ when the excitation method is changed. This effect can be seen by comparing the insets of Figures 6a and 6b. Under both excitation conditions LuAG:Gd shows the highest UV radiance. However, the radiances of the other samples are not the same. A dependency of the excitation source can be clearly seen. Here LuAG:Pr is the sample with the second largest radiance, followed by $(Gd,La)B_3O_6:Bi^{3+}$ and YAG:Pr. YAG:Gd shows the weakest emission intensity under CL excitation. We already suggested an incomplete energy transfer to the activator due to its intrinsic host luminescence,

while in the case of $(Gd,La)B_3O_6:Bi^{3+}$ the low density might be an explanation. Although YAG and LuAG have a shorter penetration depth for electron beams than the borate host due to the difference in density, we do not expect large differences in CL absorbance, because the crystal size of the particles is much larger than the penetration depth. Hence, differences in CL radiance are primarily caused by the efficiency of the energy conversion inside the phosphors.

The UV emission of Gd^{3+} as well as Pr^{3+} are well known from literature. C. W. Thiel et al., for example, investigated the systematic of 4f electron energies relative to host band levels by resonant photoemission of rare earth ions in aluminum garnets.[43]

Conclusions

The CL excited and VUV excited emission spectra of UV-B emitting phosphors reported herein were recorded and compared. All phosphors show intense emission in the UV-B spectral range upon excitation by VUV radiation or by an electron beam. The emission behavior of the samples is nearly identical under both types of
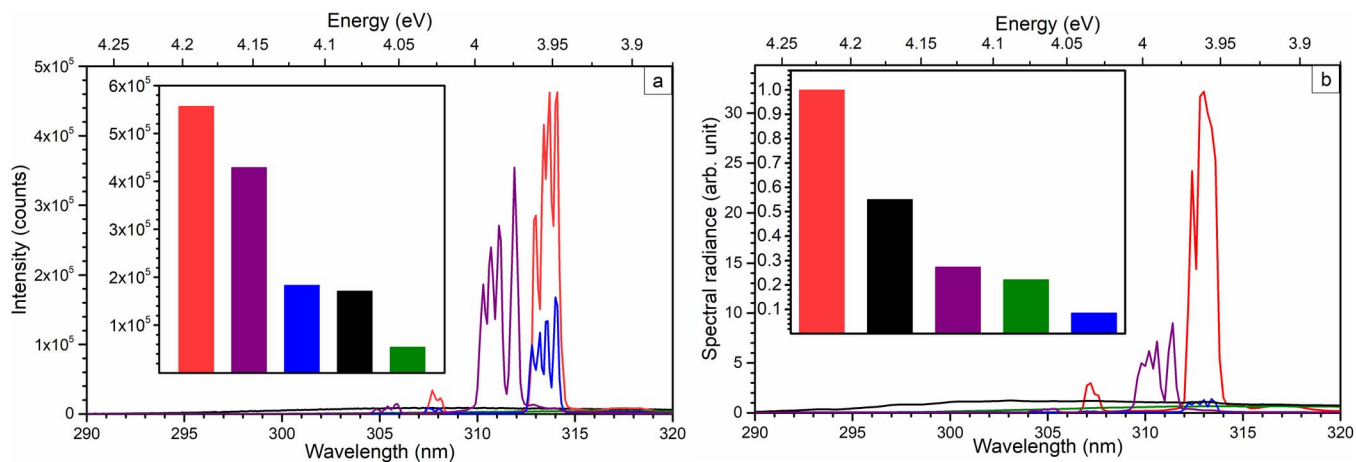
Figure 6. a) The emission spectra of $Lu_3Al_5O_{12}:Pr^{3+}$ (black line), $Lu_3Al_5O_{12}:Gd^{3+}$ (red line), $Y_3Al_5O_{12}:Pr^{3+}$ (green line), $Y_3Al_5O_{12}:Gd^{3+}$ (blue line) and $(Gd,La)B_3O_6:Bi^{3+}$ (purple line) in the range from 290 to 320 nm, under VUV (a) and cathode ray excitation (b) is shown. The inset of figure a and b the radiances (integrated intensities) of these phosphors in the UV-B range (280–320 nm) are compared using the same colors.

excitation. The Gd^{3+} doped samples manifest line emission peaking at 312 and 314 nm while the Pr^{3+} doped samples mainly show band emission in the area from 290 to 440 nm. They also show line emission in the VIS part of the spectra. This does not change when the excitation source is varied. LuAG:Gd turned out to be the material with the most intense emission in both cases. The emission intensities of the other samples are different, especially that of YAG:Gd under CL excitation. In contrast to the VUV measurements and other YAG and LuAG samples YAG:Gd was the only material in which intrinsic host luminescence could be seen under CL excitation. Moreover, the energy transfer to Gd^{3+} as well as Pr^{3+} works better in LuAG than in YAG. Due to the good emission properties of LuAG:Gd, further investigations, like temperature dependent measurements, are intended.

ORCID

Michael Laube https://orcid.org/0000-0003-3364-1552
Thomas Jansen https://orcid.org/0000-0002-6401-3746
Thomas Jüstel https://orcid.org/0000-0002-9455-5044

References

1. T. Mukai, D. Morita, M. Yamamoto, K. Akaishi, K. Matoba, K. Yasutomo, Y. Kasai, M. Sano, and S. I. Nagahama, *Physica Status Solidi (C) Current Topics in Solid State Physics*, **3**(6), 2211 (2006).
2. A. Fujioka, K. Asada, H. Yamada, T. Ohtsuka, T. Ogawa, T. Kosugi, D. Kishikawa, and T. Mukai, *Semiconductor Science and Technology*, **29**(8), 084005 (2014).
3. G. Y. Lui, D. Roser, R. Corkish, N. Ashbolt, P. Jagals, and R. Stuetz, *Science of the Total Environment*, **493**, 185 (2014).
4. N. L. Pathak and S. C. Sen, *Chemical Physics*, **7**(2), 310 (1975).
5. V. B. Bhatkar, S. K. Omanwar, and S. V. Moharil, *Optical Materials*, **29**(8), 1066 (2007).
6. G. Blasse and A. Bril, *The Journal of Chemical Physics*, **48**(1), 217 (1968).
7. M. Broxtermann, D. den Engelsen, G. R. Fern, P. Harris, T. G. Ireland, T. Jüstel, and J. Silver, *ECS Journal of Solid State Science and Technology*, **6**(4), R47 (2017).
8. G. Mandel, R. P. Bauman, and E. Banks, *The Journal of Chemical Physics*, **33**(1), 192 (1960).
9. E. Mihóková, M. Nikl, J. Pejchal, S. Baccaro, A. Cecilia, K. Nejezchleb, and A. Vedda, *physica status solidi (c)*, **4**(3), 1012 (2007).
10. D. S. Thakare, S. K. Omanwar, P. L. Muthal, S. M. Dhopte, V. K. Kondawar, and S. V. Moharil, *physica status solidi (a)*, **201**(3), 574 (2004).
11. D. S. Thakare, S. K. Omanwar, S. V. Moharil, S. M. Dhopte, P. L. Muthal, and V. K. Kondawar, *Optical Materials*, **29**(12), 1731 (2007).
12. J. A. Mares, Y. Shi, M. Nikl, Y. Shen, Y. Pan, and X. Feng, *IOP Conference Series: Materials Science and Engineering*, **15**, 012020 (2010).
13. V. Babin, K. Blazek, A. Krasnikov, K. Nejezchleb, M. Nikl, T. Savikhina, and S. Zazubovich, *physica status solidi (c)*, **2**(1), 97 (2005).
14. M. Nikl, K. Kamada, S. Kurosawa, Y. Yokota, A. Yoshikawa, J. Pejchal, and V. Babin, *physica status solidi (c)*, **10**(2), 172 (2013).
15. V. Babin, A. Krasnikov, Y. Maksimov, K. Nejezchleb, M. Nikl, T. Savikhina, and S. Zazubovich, *Optical Materials*, **30**(1), 30 (2007).
16. Y. Zorenko, A. Voloshinovskii, V. Savchyn, T. Voznyak, M. Nikl, K. Nejezchleb, V. Mikhailin, V. Kolobanov, and D. Spassky, *physica status solidi (b)*, **244**(6), 2180 (2007).
17. Y. Zorenko, V. Gorbenko, I. Konstankevych, A. Voloshinovskii, G. Stryganyuk, V. Mikhailin, V. Kolobanov, and D. Spassky, *Journal of Luminescence*, **114**(2), 85 (2005).
18. Y. Zorenko, V. Gorbenko, M. Nikl, J. A. Mares, T. Martin, and P.-A. Douissard, *IEEE Transactions on Nuclear Science*, **57**(3), 1335 (2010).
19. D. den Engelsen, P. Harris, T. Ireland, and J. Silver, *ECS Journal of Solid State Science and Technology*, **4**(2), R1 (2015).
20. D. den Engelsen, G. R. Fern, P. G. Harris, T. G. Ireland, and J. Silver, *Materials*, **10**(3), 312 (2017).
21. D. den Engelsen, G. R. Fern, T. G. Ireland, P. G. Harris, P. R. Hobson, A. Lipman, R. Dhillon, P. J. Marsh, and J. Silver, *Journal of Materials Chemistry C*, **4**(29), 7026 (2016).
22. M. Broxtermann, D. den Engelsen, G. R. Fern, P. Harris, T. G. Ireland, T. Jüstel, and J. Silver, *ECS Journal of Solid State Science and Technology*, **6**(4), R47 (2017).
23. G. Menzer, *Zeitschrift für Kristallographie - Crystalline Materials*, **69**(1–6), 300 (1929).
24. R. D. Shannon, *Acta Crystallographica Section A*, **32**(5), 751 (1976).
25. Marvin J. Weber, *Handbook of Optical Materials*, CRC Press LLC (2003).
26. V. Gorbenko, Y. Zorenko, V. Savchyn, T. Zorenko, A. Pedan, and V. Shkliarskyi, *Radiation Measurements*, **45**(3–6), 461 (2010).
27. Y. Deng, J. D. Fowlkes, J. M. Fitz-Gerald, and P. D. Rack, *Applied Physics A*, **80**(4), 787 (2005).
28. A. V. Pujats, L. M. Kuzmina, Z. A. Rachko, and J. L. Janson, *Solid State Communications*, **54**(1), 61 (1985).
29. M. Kucera, Z. Onderisinova, J. Bok, M. Hanus, P. Schauer, and M. Nikl, *Journal of Luminescence*, **169**, 674 (2016).
30. M. Nikl, A. Vedda, M. Fasoli, I. Fontana, V. V. Laguta, E. Mihokova, J. Pejchal, J. Rosa, and K. Nejezchleb, *Physical Review B*, **76**(19), 195121 (2007).
31. S. Shigeo and Y. William, M, and Y. Hajime, Eds., *Phosphor Handbook*, Second Edi. CRC Press, Boca Raton (2006).
32. M. Nikl, E. Mihokova, J. Pejchal, A. Vedda, Y. Zorenko, and K. Nejezchleb, *physica status solidi (b)*, **242**(14), R119 (2005).
33. Y. V. Zorenko, V. I. Gorbenko, G. B. Stryganyuk, V. N. Kolobanov, D. A. Spasskii, K. Blazek, and M. Nikl, *Optics and Spectroscopy*, **99**(6), 923 (2005).
34. J. Tauc, R. Grigorovici, and A. Vancu, *physica status solidi (b)*, **15**(2), 627 (1966).
35. J. Tauc, *Materials Research Bulletin*, **3**(1), 37 (1968).
36. P. Kubelka and F. Munk, *Z. Tech. Phys*, **12**(1930), 593 (1931).
37. J. E. Huheey, E. A. Keiter, and R. L. Keiter, *lnorganic Chemistry*, Prentice Hall (1992).

38. H. G. Friedmon, G. R. Choppin, and D. G. Feuerbocherz, *Journd of Chemical Education*, **41**, 354 (1964).
39. G. K. Abdullaev, K. S. Mamedov, and G. G. Dzhafarov, *Kristallografiya*, **26**(837–840), (1981).
40. A. Yoshikawa, K. Kamada, F. Saito, H. Ogino, M. Itoh, T. Katagiri, D. Iri, and M. Fujita, *IEEE Transactions on Nuclear Science*, **55**(3), 1372 (2008).
41. B. Herden, J. Nordmann, R. Komban, M. Haase, and T. Jüstel, *Optical Materials*, **35**(12), 2062 (2013).
42. B. Herden, A. Meijerink, F. T. Rabouw, M. Haase, and T. Jüstel, *Journal of Luminescence*, **146**, 302 (2014).
43. C. W. Thiel, H. Cruguel, H. Wu, Y. Sun, G. J. Lapeyre, R. L. Cone, R. W. Equall, and R. M. Macfarlane, *Physical Review B*, **64**(8), 085107 (2001).
44. S. K. Durrani, K. Saeed, A. H. Qureshi, M. Ahmad, M. Arif, N. Hussain, and T. Mohammad, *Journal of Thermal Analysis and Calorimetry*, **104**(2), 645 (2011).
45. L. Ding, Q. Zhang, J. Luo, W. Liu, W. Zhou, and S. Yin, *Journal of Alloys and Compounds*, **509**(42), 10167 (2011).